Dispersion and spectra of gravity waves probably generated by a convective storm

By A. G. KJELAAS,[1] *Norwegian Defence Research Establishment, 2007 Kjeller, Norway,*
E. E. GOSSARD, J. M. YOUNG, *NOAA/ERL, Wave Propagation Laboratory, Boulder, Colorado, USA* and W. R. MONINGER, *Coe College, Cedar Rapids, Iowa, USA*

(Manuscript received February 12, 1974)

ABSTRACT

In this paper we describe a case study of progressive gravity waves in the troposphere. We deduce their propagation speed and direction, and their dispersive characteristics, from surface spectra of wind and pressure. We compare the results with direct measurements of the waves made over an array of spaced pressure sensors using cross spectrum techniques and an algorithm developed by one of us (Young). The agreement is very satisfactory and demonstrates the feasibility of monitoring atmospheric wave conditions in almost real time using only sensors (high quality) in use at standard weather observation stations. The waves in the case we describe were highly dispersive and apparently were generated by a violent thunderstorm some 100 km west of the site of observation.

1. Introduction

Atmospheric gravity waves and convective activity are important contributors to the atmospheric pressure spectrum in the band of periods from about 1 minute to 1 hour (Gossard, 1960). The form of the spectrum of displacement of the density surfaces (or isentropes), and the dispersion characteristics of propagating disturbances reveal much about the mechanism of their generation (Gossard, 1974). In this paper we measure the spectrum and the dispersion of gravity waves apparently generated by a severe convective storm on 8 August 1972 in southeastern Colorado. The wave spectra and the dispersion of the waves we will discuss are dramatically different from the spectra and dispersion of waves analyzed by Gossard & Sweezy (1974) which they concluded were generated by dynamic instability associated with shear in the middle troposphere.

A method devised by Gossard & Sweezy (1974) will be used for determining the dispersive characteristics of the observed waves, and we will compare it with direct measurements of the speed and direction of wave components across an array of spaced pressure sensors. For the latter analysis we use the digital techniques and computer algorithm devised by one of us (Young) to carry out a cross spectral analysis between spaced sensors in such a manner that the "beam" of the array is effectively steered, or swept, continouously through 360 deg of azimuth.

In addition to the usual temporal filtering commonly used to extract mesofrequency information, we have used sensors capable of spatially filtering the atmospheric spectrum, and in this paper we will discuss the merits of such spatial filtering for sorting out the contribution of atmospheric waves for analysis. We will show that by use of such a spatial averaging of the wind field, the large mesoscale features in the wind spectrum can be effectively extracted from the turbulence "noise".

2. Analytical techniques

In the method of Gossard & Sweezy (1974), the spectra of surface pressure and wind are

[1] This paper was prepared while the senior author was a visiting scientist at the National Oceanic and Atmospheric Administration, Environmental Research Laboratories, Boulder, Colorado, under the sponsorship of the Royal Norwegian Council for Scientific and Industrial Research.

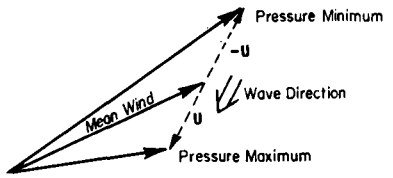

Fig. 1. Vector diagram for extracting the wind component U along the wave from fluctuations of the total wind.

combined to obtain the "spectrum" of intrinsic phase velocity of waves in the mid-frequency band of the spectra of atmospheric properties. Within the constraints of the linearized theory and the Boussinesq approximation, they point out that (e.g., see Gossard & Hooke, 1974)

$$P = \varrho_s \left(\frac{\omega}{k}\right)^2 \frac{\partial \zeta}{\partial z} \tag{1a}$$

and

$$\frac{\omega}{k} = \frac{1}{\varrho_0} \frac{P}{U}. \tag{1b}$$

In these equations

$$U, \zeta = [\varrho_0(z)/\varrho_s]^{1/2} u, \eta \quad \text{and} \quad P = [\varrho_0(z)/\varrho_s]^{-1/2} p,$$

where u, p, and η are, respectively, wave perturbations of the horizontal wind, pressure and isentropic surfaces; $\varrho_0(z)$ is the unperturbed density and ϱ_s is the density at some reference level such as the earth's surface. The wave frequency relative to an observer moving with the mean flow is ω (the intrinsic frequency) and the wavenumber $k = 2\pi/\lambda$ where λ is wavelength. Then the displacement spectrum at height H within a surface layer of constant Väisälä Brunt frequency N and constant wind is related to the pressure spectrum at the surface by

$$E_{\zeta_H}(f) = \left[\frac{H}{\varrho_s \left(\frac{\omega}{k}\right)^2}\right]^2 B^2 E_{P_0}(f) \tag{2}$$

where B is sin $n_1 H/n_1 H$ or sinh $\gamma_1 H/\gamma_1 H$ depending on whether N_1/ω is greater than or less than unity. The dispersion equation for waves of infinitesimal amplitude relating n to the wave frequency ω and wavenumber k through the Väisälä-Brunt frequency $N = \sqrt{(g/\theta)\, d\theta/dz}$ (where θ is the potential temperature) is essentially (see Gossard & Hooke, 1974)

$$n = i\gamma = k\left[\left(\frac{N}{\omega}\right)^2 - 1\right]^{1/2} \tag{3}$$

for waves whose vertical wavelength is small compared with the atmospheric scale height. Also, the relation

$$\left[\frac{\omega}{k}(f)\right]^2 = \varrho_0^{-2} \frac{E_P(f)}{E_U(f)} \tag{4}$$

provides a measure of the wave dispersion when the spectra contain an important wave contribution. The wind component U must be extracted vectorially from fluctuations of the total wind as illustrated in Fig. 1. This is accomplished by choosing a suitable numerical lowpass filter to apply to wind speed and direction, thus separating the mean wind from the total wind. The same low-pass filter is applied to the pressure record. However, our pressure sensing system had its own high-pass filter, with a time constant of 50 sec, whose effect had to be removed from the final spectrum. A low-pass numerical filter was chosen such that a perturbation of 15 min period would have its amplitude reduced to one-third the true value. The time series of wind and pressure were sampled every second and then averaged over 20 sec intervals.

Young's method of processing data from spaced sensors is to azimuthally steer the array beam in either the time or frequency domains. It differs from other algorithms such as that of Mack & Smart (1972) primarily in having greater flexibility in choice of bandwidth when signal velocity is approximately independent of frequency as in the case of acoustic waves. This is accomplished by processing in terms of the wave "slowness" (defined as the inverse of velocity) rather than processing in frequency-wavenumber space. Varying the frequency bandwidth has little influence on the average within the band when "slowness" is relatively constant over the band, so the algorithm is adaptive in choosing an optimum trade-off between confidence and spectral resolution. When applied to gravity waves, the assumption

of little dispersion is no longer necessarily valid as we shall see when results are discussed.

3. Observational techniques

The pressure sensors used in this study were essentially like that described by Bedard (1971), except that the filter amplifiers producing the various bandpasses shown in his Fig. 3 were not employed. Therefore the high frequency response was practically unlimited (as far as gravity waves are concerned) and the high-pass characteristic can be described by the single time constant of 50 sec. Each pressure sensor had 30 m of hose attached, into which hypodermic needles, used as orifices, were inserted at intervals of 1.5 m. The hose served to spatially filter out small scale turbulent inhomogeneities in the pressure field. The total pressure array consisted of a small array within a larger array as shown in Fig. 2. The small array was designed primarily to look at relatively small scale features within the boundary layer, and the large array was designed to observe larger scale features such as infrasound or long waves higher in the atmosphere. In the present study, additional spatial filtering of the pressure field was achieved by averaging pressure over the small array of sensors to obtain the spectrum of pressure for use in eqs. (2) and (4).

The anemometers used in the present study were bivanes with a high frequency response limited to approximately one Hz. However, our primary source of wind data was a unique system designed and built by G. Ochs and more completely described by Lawrence et al. (1972) and Kjelaas & Ochs (1974). The system uses a laser path to measure the average wind (somewhat weighted toward the center of the path) transverse to the path by measuring the velocity of the scintillation pattern at the receiver end. Clearly, only two such paths are needed to obtain a value of the total horizontal wind. However, the system was used in a triangular configuration so that horizontal mass convergence and divergence could be measured (Kjelaas & Ochs, 1974). This is also a suitable configuration for obtaining wind spatially averaged over the area of the triangle. The laser triangle is shown in Fig. 2.

The results of the analysis, using the spatially averaged pressure and winds as described above, were compared with results using point sensors. The advantage of using the laser winds was especially evident, and values of U obtained from bivane and from the laser triangle are shown for comparison in Fig. 5. Apparently the removal of small scale turbulence "noise" by the spatial filtering, accomplished by laser path averaging of the wind field, significantly improves the wave signal-to-noise.

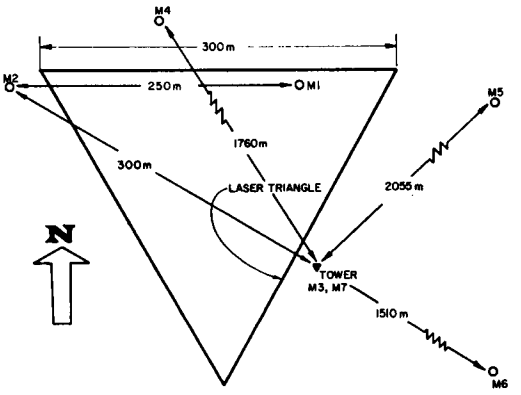

Fig. 2. Layout of the experimental configuration. The solid triangle is the laser triangle. Points marked M1, M2, M3 are the small microbarograph array, while M4, M5, M6, M7 denote the larger array. M7 is 20 m from the tower base.

4. Experimental results

The case chosen for analysis was an event which occurred in the early morning hours (0100–0230 MDT) on 8 August 1972 at Haswell, Colorado. Records of the waves of this event have been analyzed using an acoustic sounder triangle and the results published by Kjelaas et al. (1974) from whose paper the acoustic sounder records in Fig. 3, showing most of the time interval we analyzed, have been extracted. It is the purpose of our paper to analyze the dispersion and spectral characteristics using the observational techniques described above and try to deduce the mechanism of wave generation.

The pressure record and the unfiltered and low-pass filtered wind speed from the laser triangle are shown in Fig. 4. The results of carrying out the vector subtraction indicated in Fig. 1 are shown in Figs. 5 and 6. Fig. 5 shows the time series of the component U from

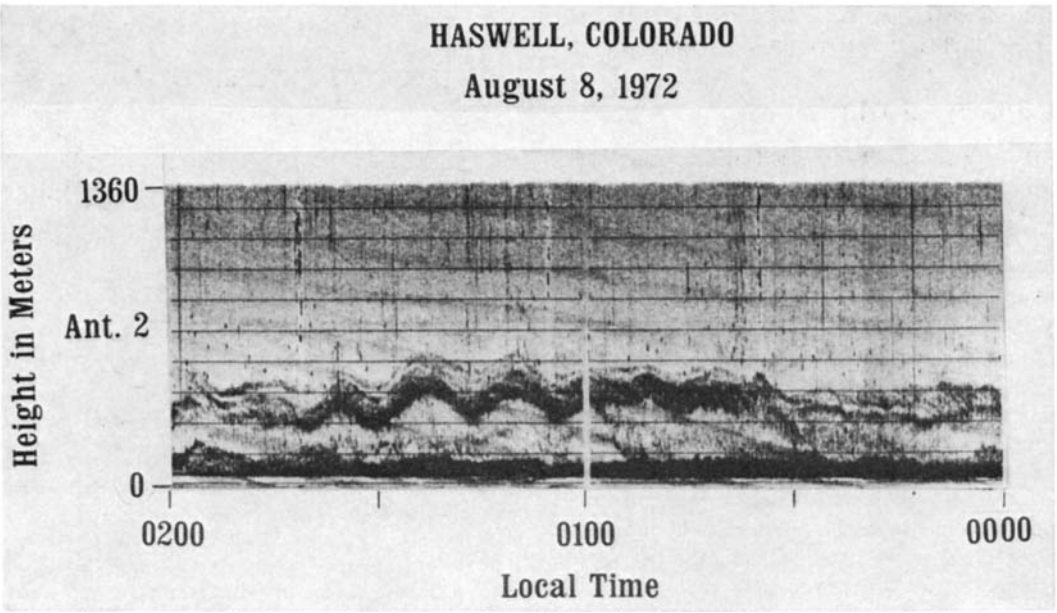

Fig. 3. Acoustic sounder record of part of the event analyzed in this paper. *LT* is Mountain Daylight Time. To convert to UT add 6 hours to LT. (From Kjelaas et al., 1974).

the laser winds along with the corresponding quantity from the bivane at 30 m elevation on a nearby tower. The fluctuating component due to the waves is much more evident in the laser wind measurements. We have chosen U as positive for clockwise rotation of the wind vector. Therefore, U and P are positively correlated when the waves come from the 180 deg sector to the left of the mean wind, but they are negatively correlated when they come from the right-hand 180 deg sector (as is the case for the principal peak in the directional distribution shown in Fig. 6). Some phase shift results from the high-pass filtering of the pressure fluctations by the pressure instrument. Fig. 6 shows the directional distribution of the waves found by the method of Gossard & Sweezy (1974). The arrows superimposed on the direction histogram show the directions obtained using Young's algorithm and the spaced array data. The arrow from 270 deg applies to the band from 21 min to 80 min, and that from 225 deg applies to the entire band from 4 to 80 min. period.

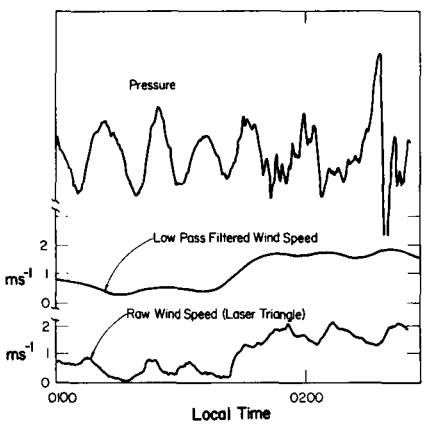

Fig. 4. Pressure recording together with the low-pass filtered and unfiltered laser wind. No scale is included for pressure since the instrument's filter characteristic has not been removed.

Fig. 7 shows the dispersion plot of phase velocity vs. frequency by the method of Gossard & Sweezy, together with the results of Young's analysis from spaced array data shown for frequency bands indicated by the bars. The spacing of elements in the array produces a high-frequency cut-off in the array spectra. The excellent agreement is a very convincing argument for the validity of both techniques. At a frequency of 2×10^{-3} Hz, the power in the spectrum (see Fig. 10) has diminished by two orders of magnitude from the peak power.

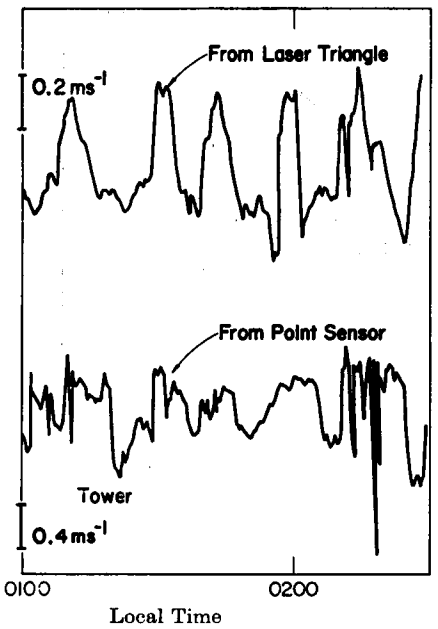

Fig. 5. Wind component U along the wave direction. Upper curve is obtained using the laser triangle, while lower curve is from the bivane at 30 m on a nearby tower.

Thus we do not consider the velocities in Fig. 7 to be significant at frequencies higher than about 2×10^{-3} Hz. During this wave event, the average surface winds were very light (about 1 m s^{-1}) and were mostly between north and east in opposition to the wave direction. We have attempted to obtain C, the true wave velocity relative to the ground, by subtracting 1 m s^{-1} from ω/k. This actually lessened the agreement in the results of the two techniques.

Fig. 8 shows the plot of ω vs. k. On this plot the slope of the line from the origin to any point on the curve represents the intrinsic phase velocity, and the slope of the tangent to the curve is the group velocity given by $d\omega/dk$.

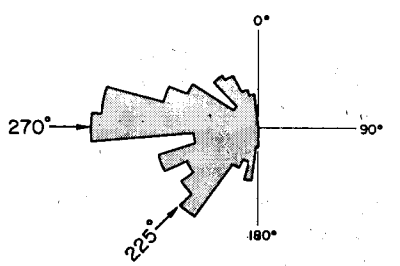

Fig. 6. Directional distribution of the waves.

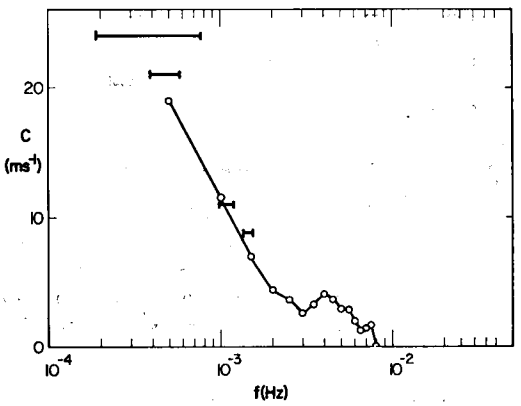

Fig. 7. Phase velocity vs. frequency. The horizontal bars are the phase velocities for different frequency bands found by applying Young's technique to the large microbarograph array. Power density of frequencies greater than $\sim 2 \times 10^{-3}$ Hz is about two orders of magnitude down from the peak in the power spectrum, so such points probably have no significance.

Fig. 9*a*, *b*, *c* shows the RAWINSONDE data obtained at 0457 MDT (the sounding nearest in time to the wave event). Unfortunately, the sounding does not well represent the lowest layers at the time of the waves, because a high surface wind sprang up at about 0400 MDT apparently due to outflow from the cool downdraft of a thundershower occurring locally at about that time. The high wind at the surface mixed the air within the radiation inversion and elevated it. We have used the surface wind and temperature data at the time of the wave event and the temperature and wind data at the top of a nearby 151 m tower (see Fig. 2)

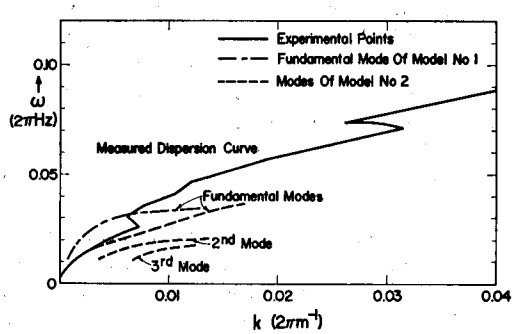

Fig. 8. Intrinsic frequency as a function of the wavenumber. Only the fundamental mode is shown for model no. 1.

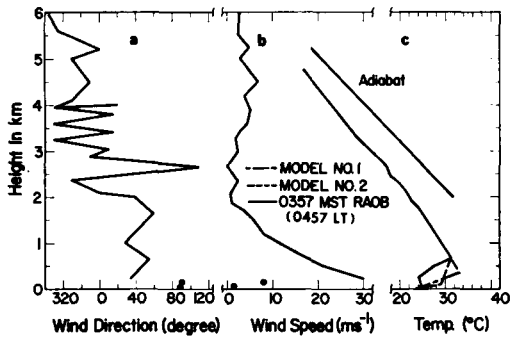

Fig. 9. Radiosonde at 0457 MDT. The circles shown are the wind and temperature data from the tower at the time of the wave event. The various atmospheric models discussed are shown as dashed curved.

to attempt to correct the sounding data back to the time of the event. The values are shown as circles, and two atmospheric models we analyze in the next section are shown as dashed and dash-dot curves in Fig. 9*c*.

Fig. 10 shows the spectrum of layer displacement at a height of 200 m calculated from eq. (2). Both the spectrum in Fig. 10 and the dispersion in Fig. 8 differ significantly from the corresponding quantities found by Gossard and Sweezy from the data taken at San Diego, Calif., under conditions of wind shear and instability aloft. The spectrum in Fig. 10 implies an r.m.s. amplitude of 38 m for the waves at a height of 200 m.

5. Comparison with models

The light winds aloft shown in Fig. 9 and the relatively low surface and tower winds at the time of the event (compared with the wave velocity of about 10 m s^{-1} at the spectrum maximum) imply that shear is not the generating mechanism for these waves. Furthermore, the waves are propagating against the background winds. Therefore it seems reasonable to compare the predictions of a shearless model with the observed dispersion.

We adopted a shearless model consisting of three layers rather than more realistic models with many layers because a three-layer model can be studied analytically whereas models with four or more layers are more effectively studied using numerical methods on high speed computers. We used a normal mode approach

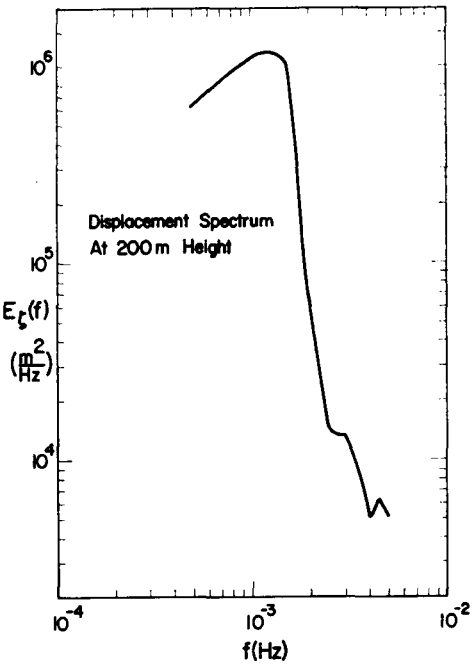

Fig. 10. Spectrum of layer displacement at a height of 200 m.

leading to an eigenvalue equation whose derivation is given by Gossard et al. (1970). They find that

$$n_2 \cot 2n_2 \Delta H = \frac{n_2^2 - n_1 \gamma_3 \cot n_1 H}{n_1 \cot n_1 H + \gamma_3} \tag{5}$$

where the subscripts apply to the three layers of a model shown schematically in Fig. 12. Eq. (5) was applied to the two models shown by the dashed and dash-dot curves in Fig. 9*c* (see caption of Fig. 12). In model no. 1 the thickness $2\Delta H$ of the middle layer is zero so it is a two-layer model for which eq. (5) becomes (see Gossard & Hooke, 1974)

$$\tan\left(kH\sqrt{\left(\frac{N_1}{\omega}\right)^2 - 1}\right) = -\frac{\sqrt{\left(\frac{N_1}{\omega}\right)^2 - 1}}{\sqrt{1 - \left(\frac{N_3}{\omega}\right)^2}}. \tag{6}$$

The resulting dispersion curves for the two models are shown plotted on Fig. 8 for comparison with the observed values. To avoid confusion from too many curves on the plot, only

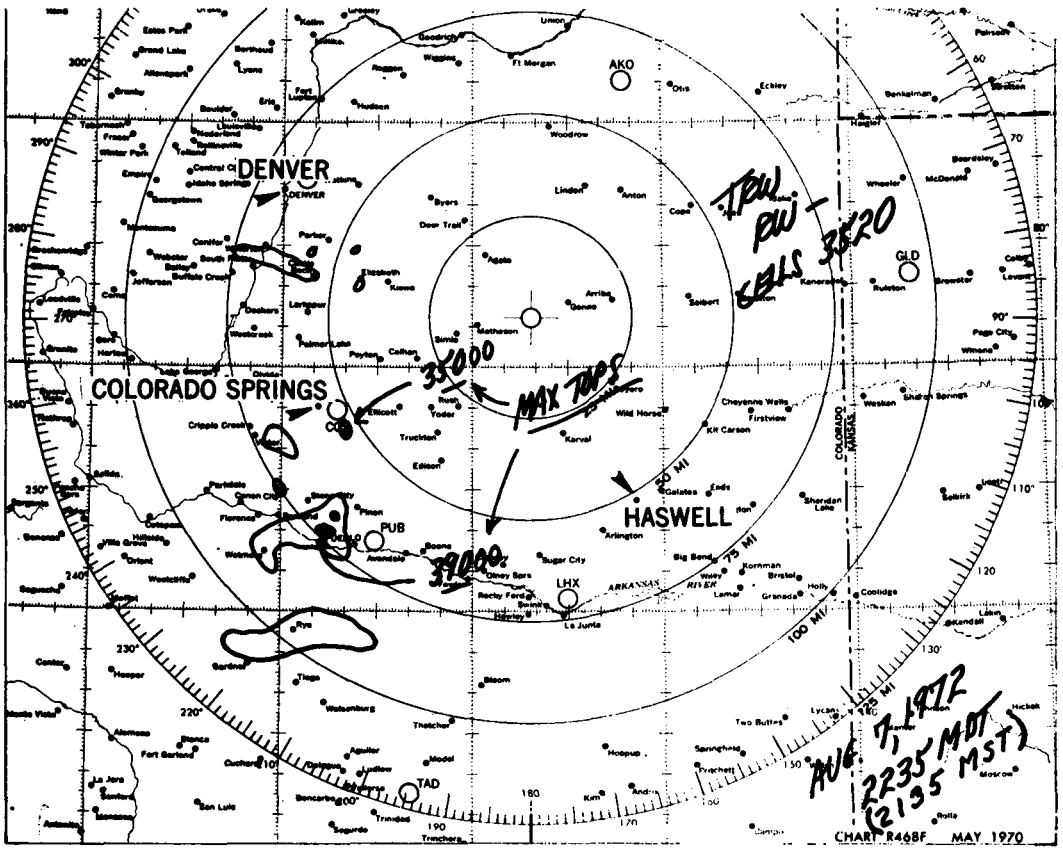

Fig. 11. Rader weather map at 2135 MST (2235 LT) obtained using the rader at Limon, Colorado.

the fundamental mode of model no. 1 has been plotted, but the second and third modes are shown for the three-layer model.

Model no. 1 provides the best fit to the gross features of the observed dispersion curve, but model no. 2 fits the low frequency portion of the curve ($\omega < 0.02$) almost exactly. In actual fact, if the waves have propagated some 100 km from the storm area, the path was undoubtedly variable, representing combinations of the various models here considered. For frequencies $\omega < N_3$, real roots to eq. (5) do not exist. This means that such waves "leak" energy upward away from the stable layers.

The important fact to note is that the observed waves are strongly dispersive as would be expected from the shearless models. If the waves had been generated by dynamic instability at a shear layer, the unstable irregularities would all travel with the mean wind speed at the center of the shear layer if the model is symmetrical with infinite upper and lower layers. If we consider a three-layer model in which the lower layer is not of infinite depth, those wave lengths long compared with its depth will no longer travel with exactly the speed of the mean wind (see Gossard, 1974), but the effect is small for the wavenumber range we consider here. The waves studied by Gossard & Sweezy (1974) displayed the non-dispersive character to be expected of wave generation by shear. The highly dispersive nature of the waves we have studied in this paper implies a different mechanism of generation. In addition, Fig. 9 shows that the shear that might have existed during the period of the event would lead to waves propagating from the northeasterly direction. They were actually propagating from the west through southwest sector (as seen in Fig. 6) with a group velocity of about 6 m s^{-1}

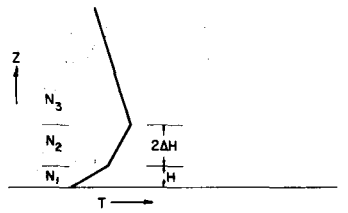

Fig. 12. The three-layer model. Model no. 1 (dash-dot curve in Fig. 8*c*) is a two-layer model, i.e., $\Delta H = 0$, in which $N_1 = 0.0354$, $N_3 = 0.0111$ and $H = 200$ m. In model no. 2 (dashed curve in Fig. 8*c*), $N_1 = 0.050$, $N_2 = 0.0202$, $N_3 = 0.0111$, $H = 100$ m, $2\Delta H = 600$ m.

at frequencies corresponding with the maximum in energy of the spectrum shown in Fig. 10. If we look 100 km to the west of Haswell on the radar weather map shown in Fig. 11 taken at 2135 MST (2235 MDT) obtained by the NWS using the WSR 57 radar at Limon, Colorado we find a violent thunderstorm near Pueblo Colorado extending above 39 000 ft (11.9 km). By 2337 MDT the tops exceeded 41 000 ft (12.5 km). It seems very likely that the waves discussed in this paper were generated by the storm. The precise mechanism is uncertain. It seems possible that the storm may act like a slow explosion in the atmosphere effectively generating the low frequency gravity waves in our example. In that case the analysis of Ramm & Warren (1963) of gravity wave generation by an impulsive source may be relevant. Note that Fig. 10 shows most of the energy to be centered at a wave period of about 14 min. On the other hand it is very possible that the cool gust front associated with the strong downdraft of the storm generated the waves in the manner of a traveling disturbance.

6. Conclusion

We conclude that the methods described in this paper and that of Gossard & Sweezy (1974) provide a useful technique for observing the properties of waves in the atmosphere and of diagnosing the probable mechanism of wave generation. The method requires only single station measurements of pressure and wind. However comparison in Fig. 5 of the wind spatially averaged over the laser triangle with measurements obtained with a point sensor emphasizes the great value of spatial filtering in the extraction of large (or meso) scale features from the turbulence dominated total wind field spectrum.

Acknowledgment

The senior author expresses his sincere gratitute to Dr C. Gordon Little Director of the Wave Propagation Laboratory for providing him with the opportunity and making the facilities available to make this study while on leave from the Norwegian Defence Research Establishment.

REFERENCES

Bedard, A. J., Jr. 1971. Seismic response of infrasonic microphones. *J. of Res. Natl. Bu. of Stand. 75C(1)*, 41–45.

Gossard, E. E. 1960. Spectra of atmospheric scalars. *J. Geophys. Res. 65*, 3339–3351.

Gossard, E. E. 1974. Dynamic stability of an isentropic shear layer in a statically stable medium. *J. Atmos. Sci. 31*(2), (in press).

Gossard, E. E., Richter, J. H. & Atlas, D. 1970. Internal waves in the atmosphere from high resolution radar measurements. *J. Geophys. Res. 75*, 903–913.

Gossard, E. E. & Hooke, W. H. 1974. *Waves in the atmosphere.* Elsevier, Amsterdam (in press).

Gossard, E. E. & Sweezy, W. B. Spectra of waves in the atmosphere (submitted to *J. Atmos. Sci.*).

Kjelaas, A. G., Beran, D. W., Hooke, W. H. & Bean, B. R. 1974. Observation of waves in the boundary-layer using an array of acoustic sounders (submitted to *J. Atmos. Sci.*).

Kjelaas, A. G. & Ochs, G. R. 1974. Study of divergence in the boundary layer using optical propagation techniques. *J. Appl. Meteorol. 13*(2), 242–248.

Lawrence, R. S., Ochs, G. R. & Clifford, S. F. 1972. The use of scintillations to measure average wind across a light beam. *Appl. Opt. 11*(2), 239–243.

Mack, H. & Smart, E. 1972. Frequency domain processing of digital microbarograph array data. *J. Geophys. Res. 77*(1), 488–490.

Ramm, P. & Warren, F. W. G. 1963. Gravity-wave dispersion under wind shear in two model atmosphere. *Q. J. R. Meteorol. Soc. 89*, 349–359.

ДИСПЕРСИЯ И СПЕКТРЫ ГРАВИТА ЦИОННЫХ ВОЛН, ВЕРОЯТНО ГЕНЕРИРУЕМЫХ КОНВЕКТИВНЫМ ШТОРМОМ

В данной статье мы описываем результаты наблюдений гравитационных волн, распространяющихся в тропосфере. Используя спектры ветра и давления, мы получаем скорости волн и направления их распространения, а также характеристики их дисперсии. Эти результаты мы сравниваем с данными прямых измерений волн, выполненными с помощью системы пространственно-разнесенных датчиков давления и обработанными с использованием техники взаимных спектров и алгоритма, разработанными одним из нас (Янгом). Согласие вполне удовлетворительное, что указывает на возможность прослеживания атмосферных волн практически в реальном времени с использованием только уже употребляемых высококачественных датчиков на стандартных станциях наблюдения за погодой. Волны в описываемом нами случае были сильно дисперсными и генерировались, очевидно, в области сильной грозы примерно в 100 *км* к западу от места наблюдения.